Chem

CellPress

Article

Multifunctional Platforms: Metal-Organic Frameworks for Cutaneous and Cosmetic Treatment

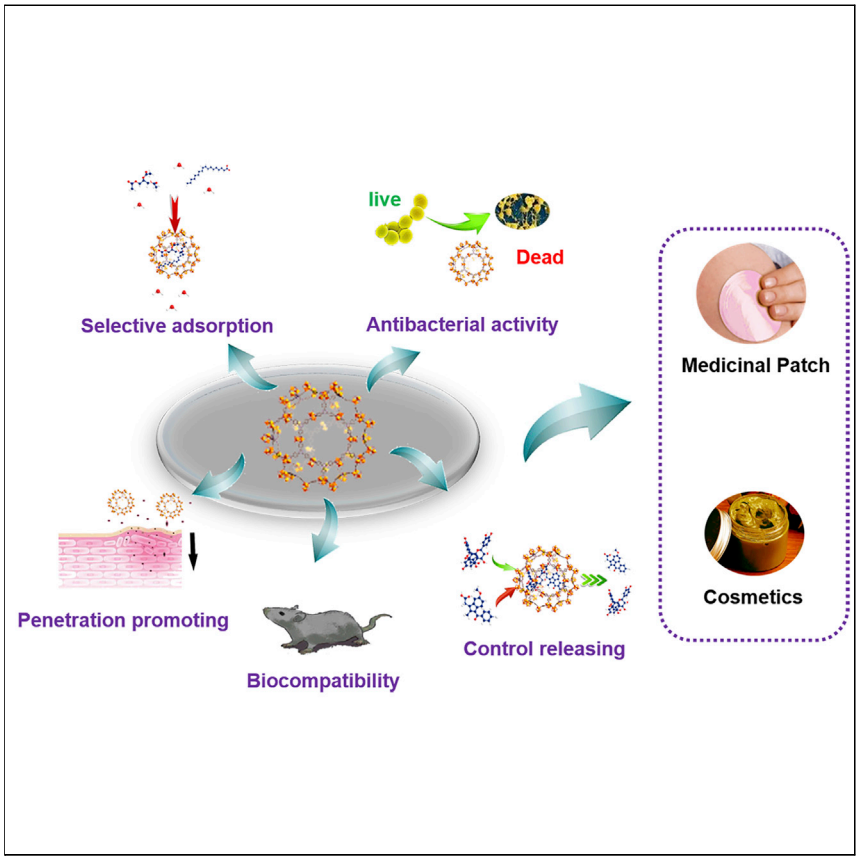

By virtue of the comprehensive assay package developed in this study, we systematically screened MOFs library for suitable materials in cutaneous and cosmetic applications and investigated the related mechanisms. Versatile and facile multifunctional (e.g., antimicrobial, control releasing, selective adsorption, and penetration promotion) platforms were constructed, and their potentials for medicinal patch and cosmetic applications were explored.

Wenjie Duan, Shan Qiao, Mingjing Zhuo, ..., Peng Cheng, Shengqian Ma, Yao Chen

Shengqian.Ma@unt.edu (S.M.)
chenyao@nankai.edu.cn (Y.C.)

HIGHLIGHTS

A systemic assay package was developed to seek MOFs for biomedical applications

Fe-based MOFs exhibited superb features that are suitable for cutaneous treatment

The relationship between MOFs' structure and their performance was in-depth analyzed

This study provides guidance to design biomedical materials for cutaneous treatment

Duan et al., Chem 7, 450–462
February 11, 2021
https://doi.org/10.1016/j.chempr.2020.11.018

CellPress

Chem

Article

Multifunctional Platforms: Metal-Organic Frameworks for Cutaneous and Cosmetic Treatment

Wenjie Duan,[1,3,7] Shan Qiao,[1,3,7] Mingjing Zhuo,[1,3] Jiaxing Sun,[1,3] Menglei Guo,[1,3] Fei Xu,[1,3] Jinjin Liu,[4] Ting Wang,[4] Xiuxiu Guo,[4] Yan Zhang,[1] Jia Gao,[4] Yueyun Huang,[5] Zhenjie Zhang,[1,4] Peng Cheng,[4] Shengqian Ma,[2,6,*] and Yao Chen[1,3,8,*]

SUMMARY

Cutaneous treatment possesses advantages, including the decrease of transient drug overdosage or systematic side effects. The evolution of biomedical materials with multifunctionalities to overcome the limitations of existing materials can bring revolutionary development in this field. A promising solution can turn to the emerging materials known as metal-organic frameworks (MOFs), featuring high porosity, easy modification, and multifunctionality. The work herein developed a systemic assay package to seek suitable MOFs for cutaneous applications. Versatile platforms based on MOFs were built, which integrated superb functions and features, including biocompatibilities, sebum adsorbability, selective adsorption, antimicrobial activity, controlled release, and skin permeability promotion. Such features endow MOFs as high-performance matrixes for cutaneous applications. This study paves a new avenue for the reformation of cosmetic and biomedicinal materials. Moreover, this comprehensive MOF screening system can be broadly applied for material evaluation in this field, which also provides valuable guidance for the design of advanced biomedical materials.

INTRODUCTION

Skin, the largest organ of our body, offers an efficient and safe route of drug administration. Cutaneous administration[1] can avoid the transient drug overdosage, can prevent drug degradation caused by hepatic first-pass metabolism, can decrease the systematic side effects, and concentrate active substances at the targeted skin lesion.[2–6] In the past several decades, cutaneous treatment has made great progress in cosmetic and pharmaceutical applications due to the advancement of biotechnology in the improvement of drug molecules.[7,8] However, the development of related materials lags far behind. The traditional biomedical materials used in cutaneous treatment often perform merely as physical supports or dispersers due to their monotonous structures and functionalities, which hinder their efficiency and application. To achieve the expected performance, additives such as a chemical enhancer,[9,10] preservative,[11] and annexing agents,[12] are usually added into cosmetics or dermatological preparations, which can raise biosafety risks, costs, and complexities for users.[13,14] Meanwhile, the most commonly used biomedical nanomaterials in cutaneous and cosmetic treatment, such as liposomes, micelles, and nanoemulsions, often have a relatively low physical stability, poor machining property, difficulty in modification/functionality, etc., which impede their broader applications in cutaneous and cosmetic treatments.[15] Therefore, developing new types of biomedicinal materials with

The Bigger Picture

Nowadays, cutaneous treatment has been widely applied in the cosmetic and pharmaceutical fields. However, traditional biomedical materials used in cutaneous treatment often showed low efficiency and limited applications due to monotonous structures and functionalities. Developing new biomedical materials with multifunctionalities and superb properties is urgently needed. Our study addresses this issue by constructing a versatile MOF-based biomedical platform, which presents multifunctionalities and avoids the introduction of unnecessary additives in preparation. More importantly, the evaluation systems developed in this study can be broadly applied for the comprehensive screening of biocompatible and multifunctional platforms in this field and provide valuable guidance for the design of advanced biomedical materials.

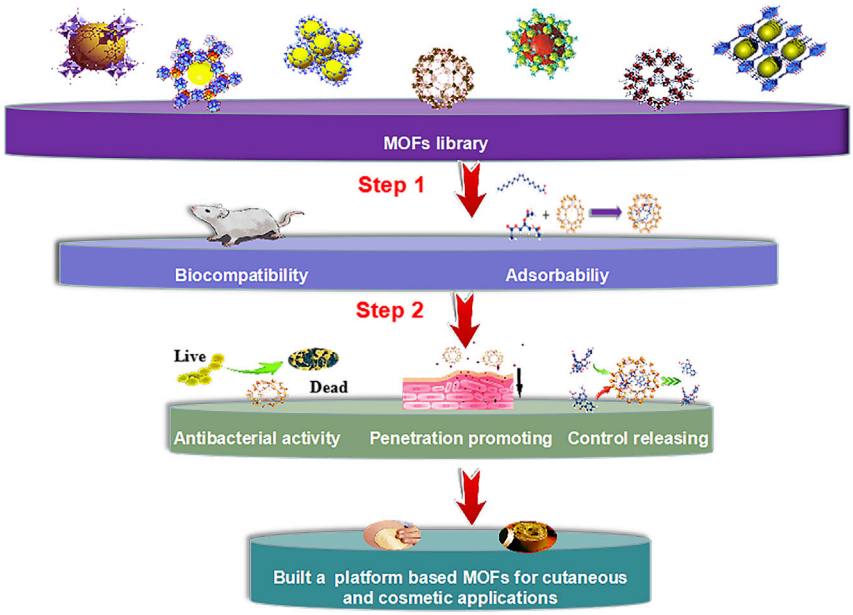

Scheme 1. Development of a Comprehensive and Efficient Assay Package for MOF-Based Cutaneous Applications.

multifunctionalities, high stability, and superb properties for cutaneous application is urgently needed.

A promising solution to address these current challenges may turn to a new class of crystalline porous materials known as metal-organic frameworks (MOFs).[16–18] MOFs feature high and tunable porosity, good physical stability and machinability, and facile post-synthetic modification.[19,20] They have exhibited excellent performance in various fields such as catalysis,[21,22] gas adsorption,[23–25] separation,[26,27] sensors,[28] and functional devices.[29] More importantly, the high structural diversity endows great amenability to design MOFs as multifunctional materials for biomedical exploration.[30–32] However, their applications in cosmetic and dermatological fields have been rarely reported. The development of MOFs for cutaneous application is a campaign of great significance, which will pave a new avenue for the improvement and reformation of materials used in this field. Herein, for the first time, we comprehensively screened MOFs library for cutaneous treatment by developing a unique and efficient assay package, and constructed versatile MOF platforms with multifunctionalities to serve for the related application and production (Scheme 1).

RESULTS AND DISCUSSION

A MOF library composed of thirteen representative MOFs (ZIF-11(Zn),[33] MIL-101(Fe),[34] MIL-101-NH_2(Fe),[35] MIL-101-CH_3(Fe), MIL-101-NO_2(Fe), MIL-101-Br(Fe), MIL-100(Fe),[36] HKUST-1(Cu),[37] MOF-808(Zr),[38] MIL-53(Al),[39] UiO-66(Zr),[40] PCN-333(Al),[41] and PCN-333(Fe)[41] was chosen due to their high water stability, low cost, easy fabrication, and high surface area. An efficient pre-evaluation was first conducted to screen the MOF library, including biocompatibility and absorbability tests. Further property investigations, such as antibacterial activity, control release, and penetration promoting were then performed to further explore their potentials for practical cutaneous applications (Scheme 1). All

[1]State Key Laboratory of Medicinal Chemical Biology, Nankai University, Tianjin 300071, China

[2]Department of Chemistry, University of North Texas, 1508 W Mulberry St, Denton, TX 76201, USA

[3]College of Pharmacy, Nankai University, Tianjin 300071, China

[4]College of Chemistry, Nankai University, Tianjin 300071, China

[5]Department of Chemistry and Chemical Engineering, Guangdong Pharmaceutical University, Guangzhou 510000, China

[6]Department of Chemistry, University of South Florida, 4202 E Fowler Avenue, Tampa, FL 33620, USA

[7]These authors contributed equally

[8]Lead Contact

*Correspondence: Shengqian.Ma@unt.edu (S.M.), chenyao@nankai.edu.cn (Y.C.)

https://doi.org/10.1016/j.chempr.2020.11.018

Table 1. The CC_{50} (μg/mL) Values for Different MOFs

	HDF	3T3	Hela
ZIF-11(Zn)	60 ± 20	60 ± 15	20 ± 9
HKUST-1(Cu)	1,140 ± 340	560 ± 160	620 ± 210
PCN-333(Fe)	7,230 ± 690	4,660 ± 220	4,430 ± 1,140
PCN-333(Al)	6,610 ± 650	3,820 ± 670	3,840 ± 740
MIL-101(Fe)	>7,200	4,920 ± 410	6,030 ± 60
MIL-101-NH_2(Fe)	>7,200	5,790± 420	5,930 ± 390
MIL-101-NO_2(Fe)	>7,200	>7,200	>6,400
MIL-101-CH_3(Fe)	>7,200	>8,400	>7,200
MIL-101-Br (Fe)	>7,200	>9,000	>8,400
MIL-100(Fe)	>7,200	>9,600	>7,200
MOF-808(Zr)	>6,400	>7,200	>7,200
UiO-66(Zr)	>7,200	>7,200	>6,400
MIL-53(Al)	>6,400	3,690 ± 450	5,160 ± 920

studied MOF samples were prepared according to the procedures reported in the literature or modified procedures. Powder X-ray diffraction (PXRD), Fourier transform infrared spectrometer (FT-IR), scanning electron microscope (SEM), thermogravimetric analysis (TGA) (Figures S1–S4) data confirmed that all MOFs possessed high crystallinity and the expected structures, as reported in the literature.

Biocompatibility is the foremost factor in biomedical and cosmetic applications, especially for the susceptible population. Therefore, the biocompatibility of selected MOFs was first evaluated. The cytotoxicity assay was conducted on human dermal fibroblasts (HDF) (Figure S5A), 3T3 (Figure S5B), and Hela (Figure S5C) cell lines. The 50% cytotoxic con1 centration (CC_{50}) values of MOFs are listed in Table 1. The cytotoxicity of MOF was inversely proportional to CC_{50} value. MIL-101(Fe) and PCN-333(Fe) were used as representatives to perform the cytotoxicity experiments with longer exposure times with cells. The results showed that there was no significant difference in cytotoxicity after incubation for 24 h compared with that of 4 h (Figures S5D–S5F). Among all the tested MOFs, Zn-based MOFs exhibited the highest cytotoxicity (ZIF-11(Zn): CC_{50} (HDF) = 60 ± 20 μg/mL; CC_{50} (Hela) = 20 ± 9 μg/mL; CC_{50} (3T3) = 60 ± 15 μg/mL), followed by Cu-based MOF (HKUST-1(Cu): CC_{50} (HDF) = 1,140 ± 340 μg/mL; CC_{50} (Hela) = 620 ± 210 μg/mL; CC_{50} (3T3) = 560 ± 160 μg/mL). The low cytotoxicity for most tested MOFs could be attributed to their relatively large particles, which prohibited cell -uptake and guaranteed their safety for cutaneous application. Overall, Fe-, Zr-, and Al-based MOFs possessed low cytotoxicity and excellent biocompatibilities, which suggest their potentials to serve as excellent transdermal matrixes.

Furthermore, hemolysis behavior for blood cells and the skin irritation test were conducted on all MOFs to further investigate their biocompatibilities. Briefly, different concentrations of MOFs were co-cultured with red blood cells (RBC) for 1, 2, and 4 h at 37°C. After centrifugation, the absorbance of the supernatant at 540 nm was measured on a microplate reader. Figures 1 and S6 show the hemolytic behavior of Fe-, Al-, Zr-, and Zn- based MOFs, which are all much lower than the clinical safety standard (5%). The hemolytic data of HKUST-1 was not successfully obtained due to its structure decomposition resulted from relatively poor water stability.[42,43] Among them, Fe-based MOFs exhibited the lowest hemolytic rate, which was lower than 3.0% even at a high concentration of 2.0 mg/mL and incubated for 4 h. These results

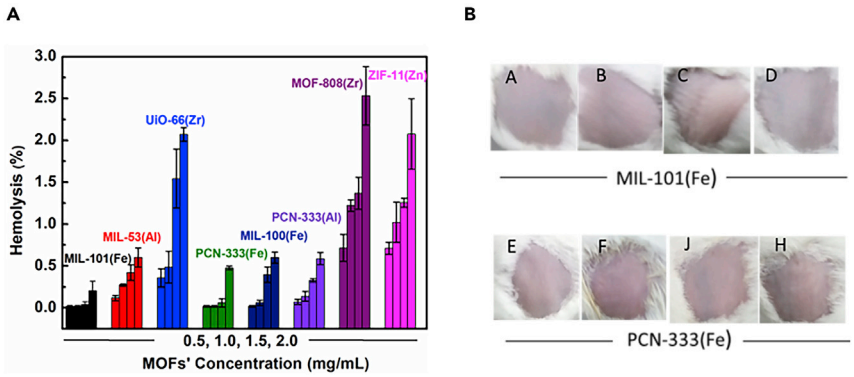

Figure 1. The Evaluation of MOFs' Biological Safety

(A) The hemolytic behavior of MOFs at different concentrations for 2 h toward RBC.

(B) The skin irritation assay results of MIL-101(Fe) and PCN-333(Fe). Pictures A and E showed the untreated mice skin. Pictures of B–D and F–G were taken after MOFs were washed away for 0, 12, and 24 h.

implied the excellent biocompatibility of Fe-based MOFs.[44] The skin irritation tests showed that the mice skin presented no erythema or edema after treating with all tested MOFs, indicating low allergenicity of the tested MOFs (Figures 1 and S7). These results, together with the cytotoxicity and hemolysis tests, implied that those MOFs exhibited good biocompatibilities, especially the Fe-based MOFs offer a higher potential to be applied in cosmetics and cutaneous treatment.

Absorbability is also a crucial factor for cutaneous applications. Excess accumulation of skin secretions will enact various pathological reactions, such as seborrheic dermatitis[45] and hircismus.[46] Additionally, the surplus sebum will affect drug delivery and transdermal process, while sebum elimination will facilitate the penetration and delivery of drugs/active compounds for therapeutic or cosmetic purposes. Therefore, the adsorption capacity of MOFs for two main dermatic secretions (triglycerides and oleic acid) were studied and compared with traditional porous materials used in cutaneous therapy or cosmetics. After encapsulation of glycerol triacetate and oleic acid, MOFs were characterized by PXRD, N_2 porosimetry, TGA, and FT-IR (Figures S8–S11), which demonstrated the successful adsorption of sebum by MOFs. The adsorption amounts of glycerol triacetate and oleic acid are summarized in Figures 2 and S12. The results indicated that all the tested MOFs possessed an excellent sorption capability for glycerol triacetate and oleic acid: 1.0 mg PCN-333(Fe) could adsorb 6.1 mg glycerol triacetate; 1.0 mg PCN-333(Fe) could adsorb 3.5 mg oleic acid, that was significantly higher than traditional porous materials (e.g., 1.0 mg active carbon can absorb 1.3 mg glycerol triacetate and 1.2 mg oleic acid). The prominent adsorption capacity of MOFs can be ascribed to the high porosity and strong interactions between organic linkers in MOFs and lipophilic molecules. In addition, the adsorption amount of oleic acid is lower than glycerol triacetate, which is probably due to the larger molecular dimension of oleic acid (glycerol triacetate: 3.2 Å × 4.8 Å × 9.6 Å, oleic acid: 3.1 Å × 8.7 Å × 16.6 Å). Notably, PCN-333(Fe) with a large pore size (42 Å and 55 Å) and high surface area (BET: 2,770 m^2/g) displayed the highest glycerol triacetate and oleic acid uptake capacity among all studied MOFs. We further investigated the influences of different structural features of MOFs on their adsorption capacities. The results demonstrated that MIL-101(Fe) variants with substituent groups, such as $-NH_2$, $-NO_2$, $-CH_3$, and -Br on terephthalate ligands, possessed higher adsorption ability compared

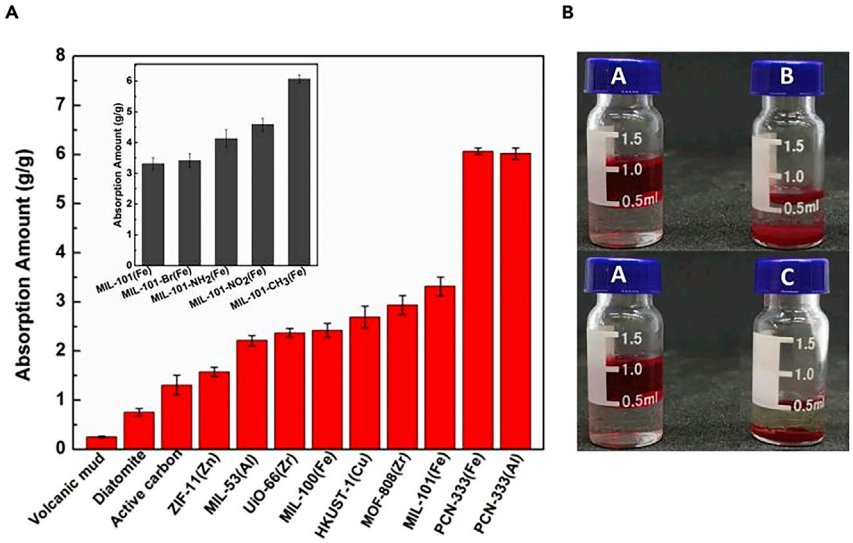

Figure 2. The Glycerol Triacetate Adsorption and Selective Adsorption Capacity of MOFs

(A) Glycerol triacetate adsorption by traditional porous materials and representative MOFs.

(B) The selective adsorption capacity of MIL-101(Fe) and PCN-333(Fe): A showed the original mixture of lipid and water in which lipid/water volume ratio is 1:1, B showed the water/lipid after selective adsorption by MIL-1010(Fe), C showed the water/lipid after selective adsorption by PCN-333(Fe).

with pristine MIL-101(Fe) (Figures 2 and S12), which could be attributed to two factors: (1) the water repellent groups (-Br, - NO_2, and -CH_3) can enhance MOFs' adsorption affinity to hydrophobic sebum; and (2) The -NH_2 group could form hydrogen bonding interaction with the functional groups in sebum molecules, such as the carbonyl group.[47,48] The results also implied that different metal centers present no significant influence on the adsorption capacity of MOFs (e.g., PCN-333(Fe) versus PCN-333(Al)).

It is preferable that materials used for cutaneous treatment can keep the skin's moisture while eliminating the excess sebum or lipid (oil).[49] Therefore, the selective adsorption capacity of MOFs toward water/triglycerides were investigated using MIL-101(Fe) and PCN-333(Fe) as representatives. These two MOFs were added to a mixture of triglycerides and water, respectively. After the removal of PCN-333(Fe), the ratio of lipid/water decreased from 1: 1 to nearly 1: 4 (Figure 2) (triglycerides were stained with Sudan IV for easy comparison), which means 80% of triglycerides were effectively removed by PCN-333(Fe), while only 20% water was adsorbed. The performance of MIL-101(Fe) was similar to PCN-333(Fe), which selectively adsorbed lipid over water. In addition, the water adsorption capacity of MOFs was carried out as a comparison. The results showed that the adsorption capacity of water was far less than that of oil (Figure S13). The results indicated that MIL-101(Fe) and PCN-333(Fe) possessed highly selective lipid adsorption capability, which can eliminate harmful skin secretion effectively without resulting in skin roughness.

The permeation of drug/active compounds through the skin (particularly stratum corneum) is a critical factor in their bioavailability. Therefore, we selected Fe-based MOFs (PCN-333 and MIL-101 series MOFs) as representatives to study their ability to promote the penetration of active molecules into the skin. The fluorescent

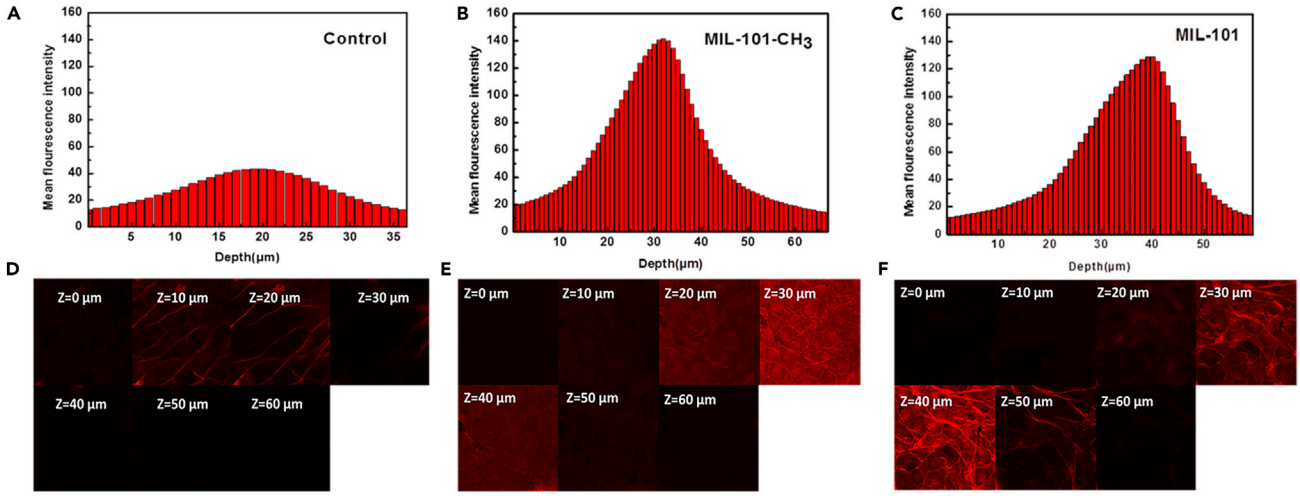

Figure 3. The Fluorescence Intensity and Graphs of Intradermal Penetration Depth of RhB into the Skin of KM Mouse

(A and D) The confocal results for skin without treatment by MOFs.

(B and E) The confocal results for skin treated by MIL-101-CH_3(Fe), the value of Z means the testing depth.

(C and F) The confocal results for skin treated by MIL-101(Fe), the value of Z means the testing depth.

rhodamine B (RhB) was used as the model molecule. The mice skin was treated with a mixture of pure MOFs and RhB-loaded MOFs for 12 h. The penetration depth of RhB was tracked with a confocal laser scanning microscope (CSLM), and the ability of MOFs to promote the penetration of RhB into the skin is directly proportional to the penetration depth and the fluorescence intensity of RhB. The results (Figure S14) revealed that the fluorescence intensity of experimental groups (skin treated with MIL-101 series) was much higher than those of the control groups, which means more RhB can penetrate skin after the treatment with MOFs. In addition, RhB in these experimental groups penetrated deeper area of skin than those in the control groups. It is notable that MIL-101(Fe) series MOFs, especially MIL-101-CH_3(Fe) and MIL-101(Fe), showed excellent ability to promote skin permeability (Figures 3 and 4). The results revealed that the ability to promote skin penetration by materials was related to their ability to adsorb sebum as well as their releasing capacity (Figure S15). A major barrier of drug penetration is the stratum corneum, which is composed of keratinocytes and lipids. Therefore, the superior adsorption capacities of MOFs can greatly facilitate skin penetration by removal of the sebum, lipid, or other wastes on the surface of the skin and expose the stratum corneum to increase its contact area with drug molecules for better penetration. The drug-releasing ability is another key factor in promoting skin penetration. For instance, MIL-101(Fe) possessed the best release performance among the tested MOFs, hence leading to good delivery performance (Figures 3 and 4). The outstanding skin-penetration promotion effect makes MOFs preeminent candidates as highly efficient transdermal matrix.

Microbes are mainly responsible for infections during cutaneous treatment or the rot of transdermal patches/cutaneous agents. Microorganisms that inhabit the skin can cause various skin diseases (e.g., dermatitis and skin ulcer).[50,51] Therefore, antibiotics or preservatives are often introduced in cosmetics or transdermal patches, which may lead to unexpected resistance, toxicity, or irritation. Herein, we investigated the antimicrobial activities of the selected MOFs to evaluate if they can inherently inhibit the growth of undesirable microbes without extra additives. *Escherichia coli* (*E. coli*), *Staphylococcus aureus* (*S. aureus*), and *Pseudomonas aeruginosa*

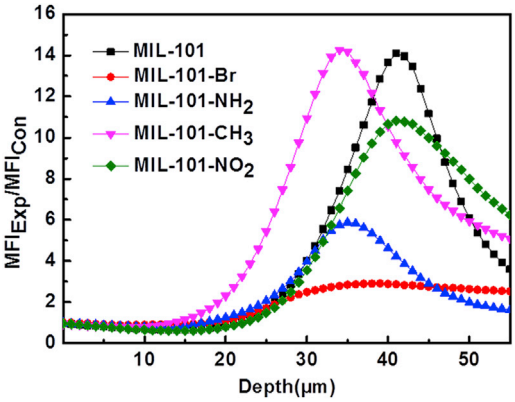

Figure 4. The Comparison Results of Permeability Promoting Capacity of MIL-101(Fe) Series MOFs.

MFIExp/MFICon = Mean fluorescence intensity of experimental group/Mean fluorescence intensity of the control group.

(*P. aeruginosa*) were used to determine the antibacterial capability of MOFs. The minimum inhibition concentration (MIC) values of MOFs are summarized in Table 2. Among all the studied MOFs, ZIF-11(Zn), HKUST-1(Cu), PCN-333(Fe), MIL-101(Fe), and MIL-101-NH_2(Fe) exhibited distinguished antimicrobial activities, especially for Gram-positive bacteria. The influence of particle sizes (Figures S23–S25) toward the antimicrobial performance of MOFs was then investigated, represented by PCN-333(Fe) and ZIF-11(Zn). The results showed that the antibacterial activity of PCN-333(Fe) and ZIF-11(Zn) with small particle sizes were higher than that with large particle sizes (Table S1). Moreover, we further investigated the solubilization speed of MOFs of different sizes through the ICP-OES (inductively coupled plasma-optical emission spectrometry) test. The results revealed that only a trace amount (<0.15%) of metal ions were exuded from MOFs after 24 h, and MOFs with a smaller size exuded more metal ions (Table S2). Therefore, it can be assumed that both the contacting possibility with bacteria and the dissolution speed of MOF particles account for the difference in antibacterial activity. Gram-positive bacteria remain an important cause of nosocomial wound infections,[52,53] and most of the superbacteria, such as MRSA (Methicillin-resistant *S. aureus*), VISA (vancomycin-intermediate *S. aureus*), and PNSP (Penicillin-nonsusceptible *S. pneumonia*) are Gram-positive bacteria. Thus, MOFs' selective antimicrobial properties provide potential for the treatment of skin diseases caused by Gram-positive bacteria. In addition, using MOFs as the multifunctional transdermal matrix can avoid the addition of antibiotics or related additives, and decrease the risk of irritation or side effect.

The high porosity and abundant interaction sites of MOFs endow them with the potentials of high loading capacity and control-releasing property. In this study, the loading capacity of MOFs (MIL-101(Fe), PCN-333(Fe)) toward procyanidine and indomethacin (two widely used active additives in skin treatment) was evaluated. We used liposome and diatomite as the control because they are common materials used in cutaneous and cosmetic treatment. As shown in Figure 5, the loading capacity of MOFs was more prominent than that of diatomite. The highly efficient loading of active compounds was further confirmed by FT-IR (Figure S16) and N_2 sorption tests (Figure S17). Meanwhile, no significant change in the PXRD patterns was observed after adsorption tests (Figure S16), indicating good stability of tested MOFs. In terms of procyanidine, the entrapment efficiency of PCN-333(Fe) and MIL-101(Fe) was 80% and 67%, and the loading capacity of PCN-333(Fe) and MIL-101(Fe) was 0.80 mg/mg and 0.67 mg/mg, respectively, which was much higher than diatomite (0.03 mg/mg) and liposome 2000 (trace). The higher loading amount

Table 2. The MIC (mg/L) Values for Different MOFs

	Staphylococcus aureus	*Escherichia coli*	*Pseudomonas aeruginosa*
ZIF-11(Zn)	150	180	350
HKUST-1(Cu)	400	>1,000	>1,000
PCN-333(Fe)	300	560	450
PCN-333(Al)	>360	>1,000	>1,000
MIL-101(Fe)	300	>630	500
MIL-101-NH_2(Fe)	280	>620	430
MIL-101-NO_2(Fe)	>600	>900	>900
MIL-101-CH_3(Fe)	>650	>900	>900
MIL-101-Br(Fe)	>700	>900	>900
MIL-100(Fe)	>360	>630	>620
MOF-808(Zr)	>810	>1,000	>1,000
UiO-66(Zr)	>720	>1,000	>1,000

of PCN-333(Fe) than MIL-101(Fe) may be correlated with the higher surface area and the larger window/pore size of PCN-333(Fe) (Table S3). The low loading capacity of diatomite can be attributed to the lack of organic groups to provide interactions with guest molecules as well as its low surface area (BET ~23 m^2/g).[54] The influence of particle sizes of MOFs toward their adsorption capacities and rates was also investigated, and the result showed that MIL-101 with a smaller particle size was superior to that with a larger particle size (Figure S18). In order to evaluate the controlled release kinetics, we tracked the amounts of the released active compounds from MOFs at different time frames. As shown in Figure 5, PCN-333(Fe) completely released procyanidine and indomethacin after ~120 and 130 h, respectively. For MIL-101(Fe), 72% of procyanidine and 60% of indomethacin could be released after ~130 and 100 h. MIL-101(Fe)'s slow release mainly resulted from its small window sizes (~12 Å and 15 Å)[34] compared with PCN-333(Fe) (26 Å and 30 Å).[41] The interactions between MOFs and guest compounds are responsible for the controlled release, which avoid the "burst release effect" related to side effects and provide better bioavailability of active substances. Overall, the high loading capacities and controlled releasing properties of MOFs make them a promising efficient matrix in cutaneous or cosmetics applications (e.g., sleeping masks, perfume, burn ointment).

After a comprehensive evaluation, Fe-based MOFs, especially MIL-101(Fe), demonstrated the highest potential to serve as a multifunctional platform for cutaneous treatment. On the one hand, the good biocompatibility, high stability (Figures S19–S21; Table S3), and excellent absorbability guarantees them as reliable and efficient cutaneous applications. On the other hand, several superb features such as antimicrobial activity, control-releasing capability, and satisfactory promotion to penetration entitle them as a versatile platform to facilitate an enhanced bioavailability of active substances without extra additives (e.g., chemical enhancers, release liner, and preservatives). Moreover, the relatively low cost of reagents (e.g., terephthalate and Fe salts) and easy large-scale synthesis make MIL-101(Fe) the most promising material for applications, including fine chemicals, cosmetics, and transdermal matrix. The facile functionality of MOFs further promotes them as potential platforms that can be customized to meet specific requirements for distinct active molecules in dermatological preparations and cosmetics. Finally, to demonstrate the practical application of MOFs in cosmetics, a peeling cleaning facial mask was fabricated using Fe-based MOFs (Figure S22). The development of other MOF-based functional cosmetics and transdermal

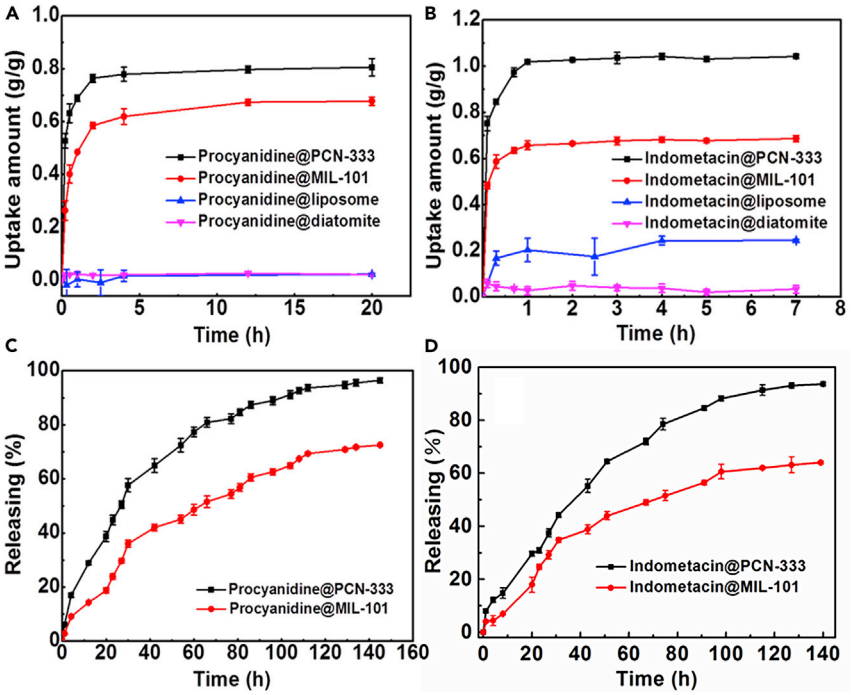

Figure 5. The Uptake and Release Profile of MOFs to the Active Substance

(A) The uptake profile of procyanidine into MIL-101(Fe) (red), PCN-333(Fe) (black), liposome(blue), and diatomite (purple).

(B) The uptake profile of indomethacin into MIL-101(Fe) (red), PCN-333(Fe) (black), liposome(blue), and diatomite (purple).

(C) The releasing profile of procyanidine from PCN-333(Fe) (black) and MIL-101(Fe) (red).

(D) The releasing profile of indomethacin from PCN-333(Fe) (black) and from MIL-101(Fe) (red).

patch, and the formula optimization for commercial products is ongoing in our lab.

CONCLUSIONS

In conclusion, for the first time, we developed a systematic assay package to efficiently evaluate MOFs for cutaneous and cosmetic applications, based on which we built versatile and facile MOFs platforms that exhibit excellent biocompatibilities, high sebum adsorption, selective adsorption capacity, antimicrobial activity, skin permeability promotion, and control-release property. These great properties make MOFs ideal candidates to serve as high-performance matrixes for cutaneous applications, such as dermatological preparations and cosmetics. Further analysis of the structure-activity relationship of MOFs guided an in-depth understanding of the principles for the rational design of high-performance functional materials for cutaneous treatment. The results revealed that metal irons have a direct effect on the biocompatibilities of corresponding MOFs, while the ligands, especially their functional groups, are closely related to MOFs functionality and performance, such as selective adsorption and promotion of skin penetration. This study will pave a new avenue for the design, synthesis, and application of multifunctional biomedical materials. More importantly, the comprehensive MOFs screening system developed in this study can be broadly applied for material evaluation in cutaneous and cosmetic treatment and provide valuable guidance for the rational design of advanced biomedical materials.

EXPERIMENTAL PROCEDURES

Resource Availability

Lead Contact

Further information and requests for resources should be directed to and will be fulfilled by the Lead Contact, Yao Chen (chenyao@nankai.edu.cn).

Materials Availability

This study did not generate new unique reagents.

Data and Code Availability

This study did not generate any datasets.

Cytotoxicity Assay

The cytotoxicity experiment was referred to the operation procedure reported in the literature.[55–57] HDF cells and 3T3 cells were cultured in DMEM medium (high glucose, GIBCO), Hela cells were cultured in RPMI-1640 medium, which was supplemented with 10% of heat-inactive fetal bovine serum (FBS; PAN) and 1% of antibiotic (Penicillin streptomycin) at 37°C in the incubator with 5% CO_2. The cytotoxicity of MOFs was evaluated via 3-(4,5-dimethylthiazol-2-yl)-2,5-diphenytetrazolium bromide (MTT; Beyotime) assay. The cells were seeded in 96-well plates at a desirable density (~5 × 10^4 cells/mL) and cultured overnight. MOFs were pre-grinded and then dispersed in the aqueous medium. Ultrasonic treatment was then conducted to generate a uniform suspension before applying it to cell wells. Then the various concentrations of MOFs suspensions were added into cells and incubated for 4 h. MTT solutions (10 μL; 5 mg/mL) and 100 μL medium were then added to each well and incubated for 4 h at 37°C with a 5% CO_2 atmosphere. The medium was removed and 100 μL DMSO (Sigma) was added to each well. The plate was read at λ = 490 nm.

Hemolysis Assay

Various amounts of MOFs were dispersed in PBS buffer. Subsequently, 450 μL of 4% RBCs was added to 50 μL MOF suspension and incubated at 37°C.[58] After 1, 2, and 4 h, the solution was centrifuged, and the supernatants were scanned at 540 nm on a microplate reader. PBS buffer (+RBCs) and 1% Triton-X-100 (+RBCs) were used as the negative and positive controls, respectively. Blood-cell mortality or hemolysis rate = (sample 540nm − negative control 540nm) / (positive control 540nm − negative control 540nm) × 100%.

Animal Test

The animal study protocols were referred to a reported method.[58] KM mice (8-week old), which were randomly grouped (half male and half female) were selected to perform the animal test. The mice were depilated (about 4 cm × 4 cm) on both sides of the back. The left side of each mouse without any treatment was chosen as the control side. The right side was chosen as the experimental side, and MOFs samples were applied (100 mg/mL) on the surface of the skin and fixed with tape on it. After 2 h, the samples were washed away with water. The photos of the mice skin were taken after 0, 12, and 24 h of the treatment.

Sebum Adsorption Capacity

In the 20 mL glass vials, 0.20 g of MOFs were introduced into 10.0 mL of triglycerides or oleic acid. After stirring at 37°C for 20 min, the mixture was filtrated with a filter membrane (0.22 μm), and then washed with ethanol to remove the sebum adhered

on MOFs surface. The adsorption quantity of sebum by different MOFs was obtained via comparing weight variations between pristine MOFs and oil@MOFs.

Selective Adsorption Test

In a 2.0 mL vial, 0.5 mL of DI water and 0.5 mL of triglycerides were mixed. Subsequently, 70.0 mg PCN-333(Fe) was introduced to the mixture and stirred for 10 min. After MOFs were removed by filtration, the water-oil mixture was fully stratified. The remaining liquid mixture was stained with Sudan IV for easy visualization and comparison. Thus, we measured the volume of the residual oil and water, and quantitatively calculated uptake of water and oil by MOFs. The control group without MOFs was also treated in the same procedure.

Minimum Inhibition Concentration Assay

The antibacterial activities of MOFs were analyzed using the method described by Fiebelkorn et al.[59] The experimental strains were inoculated into a 50 mL medium to culture overnight at 37°C. Then the bacterial suspension was added into all tubes at a desirable density. Different concentrations of MOFs were dispersed in the sterilized LB medium and then added to the tubes. Control groups were performed without MOFs. All the tubes were cultured for 48 h at 37°C. The concentration of bacteria under different treatments was determined at 600 nm at a different time frame.

Encapsulation of Active Compounds and Control-Release Study

Generally, 50 mg of activated MOFs were dispersed into 10.0 mL indomethacin ethanol solution (20 mg/mL) or procyanidine aqueous solution (5 mg/mL) and stirred.[60] Then, the concentration of supernatants was monitored at a certain time interval using UV spectrometer (λ = 320 nm for indomethacin; λ = 280 nm for procyanidine). The standard adsorption curves were determined at the same wavelength with different concentrations. To remove the surface-adsorbed guest molecules, the saturated MOFs (with active compounds) were washed with water and monitored by UV absorption. To investigate the release profile of active compounds from MOFs, 90 mg procyanidine@PCN-333(Fe) and 84 mg procyanidine@MIL-101(Fe) were immersed into 10 mL PBS at 37°C, and 103 mg indometacin@PCN-333(Fe) and 84 mg indometacin@MIL-101(Fe) immersed into 10 mL ethanol at 37°C (indomethacin is insoluble in PBS). The concentration of the released active substance in the supernatant was determined with the same procure mentioned in the encapsulation process. The entrapment efficiency (%EE) and the loading capacity (LC, g/g) were calculated as follows:

$$\text{Entrapment efficiency (\%EE)} = \frac{\text{weight of drug in MOFs}}{\text{weight of drug fed initially}} \times 100\%$$

$$\text{Loading capacity(LC)} = \frac{\text{weight of drug in MOFs}}{\text{weight of materials}}$$

Skin Permeation Assay

The dorsal skin samples of 6-week old male mice (KM) were selected to perform the skin permeation assay. The skin-penetration depth was viewed with a confocal laser scanning microscope (CLSM) through the Z axis. The dorsal skin samples were placed on the surface of a home-made Franz diffusion chamber.[61] A mixture of pure MOFs and RhB-loaded MOFs (ratio = 5/3) was added to the cuticle of the dorsal skin and was incubated for 12 h at 37°C. As a control, 30 μL rhodamine B (1 mg/mL, so the applied amount of free RhB was close to the RhB from MOF samples) was added and then incubated under the same conditions. After that, the MOFs loaded with RhB and excess fluorescent dye was removed by wiping the skin with the swab. The skin samples were then transferred to the glass slides, and the depth of RhB into

the skin was viewed by CLSM using exciting light at 561 nm and emitting light at 625 nm.

SUPPLEMENTAL INFORMATION

Supplemental Information can be found online at https://doi.org/10.1016/j.chempr.2020.11.018.

ACKNOWLEDGMENTS

The authors acknowledge financial support from the National Key Research and Development Program of China (2018YFA0901800), the National Natural Science Foundation of China (21871153 and 31800793), and the Tianjin Natural Science Foundation of China (18JCZDJC37300). Partial support from the Robert A. Welch Foundation (B-0027) is also acknowledged (S.M.).

AUTHOR CONTRIBUTIONS

Y.C., Z.Z., and S.M. conceived and directed the project. W.D., S.Q. designed and carried out the experiments. All authors discussed the results and wrote the paper.

DECLARATION OF INTERESTS

The authors declare no competing financial interests.

Received: November 22, 2019
Revised: December 30, 2019
Accepted: November 16, 2020
Published: December 9, 2020

REFERENCES

1. Prausnitz, M.R., and Langer, R. (2008). Transdermal drug delivery. Nat. Biotechnol. *26*, 1261–1268.
2. Ita, K.B. (2014). Transdermal drug delivery: progress and challenges. J. Drug Deliv. Sci. Technol. *24*, 245–250.
3. Xie, Y., Xu, B., and Gao, Y. (2005). Controlled transdermal delivery of model drug compounds by MEMS microneedle array. Nanomedicine *1*, 184–190.
4. Prausnitz, M.R., Mitragotri, S., and Langer, R. (2004). Current status and future potential of transdermal drug delivery. Nat. Rev. Drug Discov. *3*, 115–124.
5. Langer, R. (2001). Drug delivery. Drugs on target. Science *293*, 58–59.
6. Hayes, B.D., Klein-Schwartz, W., Clark, R.F., Muller, A.A., and Miloradovich, J.E. (2010). Comparison of toxicity of acute overdoses with citalopram and escitalopram. J. Emerg. Med. *39*, 44–48.
7. Sloan, K.B., and Wasdo, S. (2003). Designing for topical delivery: prodrugs can make the difference. Med. Res. Rev. *23*, 763–793.
8. Sloan, K.B., Wasdo, S.C., and Rautio, J. (2006). Design for optimized topical delivery: prodrugs and a paradigm change. Pharm. Res. *23*, 2729–2747.
9. Haq, A., and Michniak-Kohn, B. (2018). Effects of solvents and penetration enhancers on transdermal delivery of thymoquinone: permeability and skin deposition study. Drug Deliv. *25*, 1943–1949.
10. Ita, B.K. (2015). Chemical penetration enhancers for transdermal drug delivery-success and challenges. Drug Deliv. *12*, 645–651.
11. Orton, D.I., and Wilkinson, J.D. (2004). Cosmetic allergy. Am. J. Clin. Dermatol. *5*, 327–337.
12. Gupta, R., Sridhar, D.B., and Rai, B. (2016). Molecular Dynamics simulation study of permeation of molecules through skin lipid bilayer. J. Phys. Chem. B. *120*, 8987–8996.
13. Ita, K.B. (2014). Transdermal drug delivery: progress and challenges. J. Drug Deliv. Sci. Technol. *24*, 245–250.
14. Howell-Jones, R.S., Wilson, M.J., Hill, K.E., Howard, A.J., Price, P.E., and Thomas, D.W. (2005). A review of the microbiology, antibiotic usage and resistance in chronic skin wounds. J. Antimicrob. Chemother. *55*, 143–149.
15. Sercombe, L., Veerati, T., Moheimani, F., Wu, S.Y., Sood, A.K., and Hua, S. (2015). Advances and challenges of liposome assisted drug delivery. Front. Pharmacol. *6*, 286.
16. Zhou, H.C., and Kitagawa, S. (2014). Metal–organic frameworks (MOFs). Chem. Soc. Rev. *43*, 5415–5418.
17. Maurin, G., Serre, C., Cooper, A., and Férey, G. (2017). The new age of MOFs and of their porous-related solids. Chem. Soc. Rev. *46*, 3104–3107.
18. Cui, Y., Li, B., He, H., Zhou, W., Chen, B., and Qian, G. (2016). Metal–organic frameworks as platforms for functional materials. Acc. Chem. Res. *49*, 483–493.
19. Furukawa, H., Cordova, K.E., O'Keeffe, M., and Yaghi, O.M. (2013). The chemistry and applications of metal-organic frameworks. Science *341*, 1230444.
20. Burrows, A.D., Frost, C.G., Mahon, M.F., and Richardson, C. (2008). Post-synthetic modification of tagged metal–organic frameworks. Angew. Chem. Int. Ed. Engl. *47*, 8482–8486.
21. García-García, P., Müller, M., and Corma, A. (2014). MOF catalysis in relation to their homogeneous counterparts and conventional solid catalysts. Chem. Sci. *5*, 2979–3007.
22. Jiao, L., Wang, Y., Jiang, H.L., and Xu, Q. (2018). Metal–organic frameworks as platforms for catalytic applications. Adv. Mater. *30*, 1703663.
23. Li, H., Wang, K., Sun, Y., Lollar, C.T., Li, J., and Zhou, H.C. (2018). Recent advances in gas storage and separation using metal–organic frameworks. Mater. Today *21*, 108–121.
24. Li, J.R., Yu, J., Lu, W., Sun, L.B., Sculley, J., Balbuena, P.B., et al. (2013). Porous materials with pre-designed single-molecule traps for

CO_2 selective adsorption. Nat. Commun. *4*, 1538.

25. Xiang, S., He, Y., Zhang, Z., Wu, H., Zhou, W., Krishna, R., and Chen, B. (2012). Microporous metal-organic framework with potential for carbon dioxide capture at ambient conditions. Nat. Commun. *3*, 954.

26. Rodenas, T., Luz, I., Prieto, G., Seoane, B., Miro, H., Corma, A., Kapteijn, F., Llabrés I Xamena, F.X., and Gascon, J. (2015). Metal–organic framework nanosheets in polymer composite materials for gas separation. Nat. Mater. *14*, 48–55.

27. Xiang, S.C., Zhang, Z., Zhao, C.G., Hong, K., Zhao, X., Ding, D.R., Xie, M.H., Wu, C.D., Das, M.C., Gill, R., et al. (2011). Rationally tuned micropores within enantiopure metal-organic frameworks for highly selective separation of acetylene and ethylene. Nat. Commun. *2*, 204.

28. Liu, X., Qi, W., Wang, Y., Su, R., and He, Z. (2017). A facile strategy for enzyme immobilization with highly stable hierarchically porous metal–organic frameworks. Nanoscale *9*, 17561–17570.

29. Ma, H., Liu, J., Ali, M.M., Mahmood, M.A.I., Labanieh, L., Lu, M., Iqbal, S.M., Zhang, Q., Zhao, W., and Wan, Y. (2015). Nucleic acid aptamers in cancer research, diagnosis and therapy. Chem. Soc. Rev. *44*, 1240–1256.

30. Chen, Y., Lykourinou, V., Vetromile, C., Hoang, T., Ming, L.J., Larsen, R.W., and Ma, S. (2012). How can proteins enter the interior of a MOF? Investigation of cytochrome c translocation into a MOF consisting of mesoporous cages with microporous windows. J. Am. Chem. Soc. *134*, 13188–13191.

31. Wang, Z., Hu, S., Yang, J., Liang, A., Li, Y., Zhuang, Q., and Gu, J. (2018). Nanoscale Zr-based MOFs with tailorable size and introduced mesopore for protein delivery. Adv. Funct. Mater. *28*, 1707356.

32. Horcajada, P., Gref, R., Baati, T., Allan, P.K., Maurin, G., Couvreur, P., Férey, G., Morris, R.E., and Serre, C. (2012). Metal-organic frameworks in biomedicine. Chem. Rev. *112*, 1232–1268.

33. Park, K.S., Ni, Z., Côté, A.P., Choi, J.Y., Huang, R., Uribe-Romo, F.J., Chae, H.K., O'Keeffe, M., and Yaghi, O.M. (2006). Exceptional chemical and thermal stability of zeolitic imidazolate frameworks. Proc Natl. Acad. Sci. U.S.A. *103*, 10186–10191.

34. Férey, G., Mellot-Draznieks, C., Serre, C., Millange, F., Dutour, J., Surblé, S., and Margiolaki, I. (2005). A chromium terephthalate-based solid with unusually large pore volumes and surface area. Science *309*, 2040–2042.

35. Bauer, S., Serre, C., Devic, T., Horcajada, P., Marrot, J., Férey, G., and Stock, N. (2008). High-throughput assisted rationalization of the formation of metal organic frameworks in the iron (III) aminoterephthalate solvothermal system. Inorg. Chem. *47*, 7568–7576.

36. Férey, G., Serre, C., Mellot-Draznieks, C., Millange, F., Surblé, S., Dutour, J., and Margiolaki, I. (2004). A hybrid solid with giant pores prepared by a combination of targeted chemistry, simulation, and powder diffraction. Angew. Chem. Int. Ed. Engl. *43*, 6296–6301.

37. Chui, S.S.Y., Lo, S.M.F., Charmant, J.P., Orpen, A.G., and Williams, I.D. (1999). A chemically functionalizable nanoporous material. Science *283*, 1148–1150.

38. Liang, W., Chevreau, H., Ragon, F., Southon, P.D., Peterson, V.K., and D'Alessandro, D.M. (2014). Tuning pore size in a zirconium–tricarboxylate metal–organic framework. CrystEngComm *16*, 6530–6533.

39. Serre, C., Millange, F., Thouvenot, C., Noguès, M., Marsolier, G., Louër, D., and Férey, G. (2002). Very large breathing effect in the first nanoporous chromium (III)-based solids: MIL-53 or CrIII (OH)·x [O2C- C6H4-CO2] x [HO2C-C6H4-CO2H]x·x H2Oy. J. Am. Chem. Soc. *124*, 13519–13526.

40. Cavka, J.H., Jakobsen, S., Olsbye, U., Guillou, N., Lamberti, C., Bordiga, S., and Lillerud, K.P. (2008). A new zirconium inorganic building brick forming metal organic frameworks with exceptional stability. J. Am. Chem. Soc. *130*, 13850–13851.

41. Feng, D., Liu, T.F., Su, J., Bosch, M., Wei, Z., Wan, W., Yuan, D., Chen, Y.P., Wang, X., Wang, K., et al. (2015). Stable metal-organic frameworks containing single-molecule traps for enzyme encapsulation. Nat. Commun. *6*, 5979.

42. Álvarez, J.R., Sánchez-González, E., Pérez, E., Schneider-Revueltas, E., Martínez, A., Tejeda-Cruz, A., et al. (2017). Structure stability of HKUST-1 towards water and ethanol and their effect on its CO_2 capture properties. Dalton Trans. *46*, 9192–9200.

43. DeCoste, J.B., Peterson, G.W., Schindler, B.J., Killops, K.L., Browe, M.A., and Mahle, J.J. (2013). The effect of water adsorption on the structure of the carboxylate containing metal–organic frameworks Cu-BTC, Mg-MOF-74, and UiO-66. J. Mater. Chem. A *1*, 11922–11932.

44. Grall, R., Hidalgo, T., Delic, J., Garcia-Marquez, A., Chevillard, S., and Horcajada, P. (2015). In vitro biocompatibility of mesoporous metal (III; Fe, Al, Cr) trimesate MOF nanocarriers. J. Mater. Chem. *3*, 8279–8292.

45. Paulino, L.C. (2017). New perspectives on dandruff and seborrheic dermatitis: lessons we learned from bacterial and fungal skin microbiota. Eur. J. Dermatol. *27*, 4–7.

46. Shokry, E., de Oliveira, A.E., Avelino, M.A.G., de Deus, M.M., and Filho, N.R.A. (2017). Earwax: A neglected body secretion or a step ahead in clinical diagnosis? A pilot study. J. Proteomics *159*, 92–101.

47. Hansch, C., Leo, A., Unger, S.H., Kim, K.H., Nikaitani, D., and Lien, E.J. (1973). Aromatic substituent constants for structure-activity correlations. J. Med. Chem. *16*, 1207–1216.

48. Seo, P.W., Bhadra, B.N., Ahmed, I., Khan, N.A., and Jhung, S.H. (2016). Adsorptive removal of pharmaceuticals and personal care products from water with functionalized metal-organic frameworks: remarkable adsorbents with hydrogen-bonding abilities. Sci. Rep. *6*, 34462.

49. Musthaq, S., Mazuy, A., and Jakus, J. (2018). The microbiome in dermatology. Clin. Dermatol. *36*, 390–398.

50. Nakatsuji, T., Chen, T.H., Narala, S., Chun, K.A., Two, A.M., Yun, T., et al. (2017). Antimicrobials from human skin commensal bacteria protect against *Staphylococcus aureus* and are deficient in atopic dermatitis. Sci. Transl. Med. *9*, eaah4680.

51. Lei, X., Liu, B., Huang, Z., and Wu, J. (2015). A clinical study of photodynamic therapy for chronic skin ulcers in lower limbs infected with *Pseudomonas aeruginosa*. Arch. Dermatol. Res. *307*, 49–55.

52. Grice, E.A., and Segre, J.A. (2011). The skin microbiome. Nat. Rev. Microbiol. *9*, 244–253.

53. Bunce, C., Wheeler, L., Reed, G., Musser, J., and Barg, N. (1992). Murine model of cutaneous infection with Gram-positive cocci. Infect. Immun. *60*, 2636–2640.

54. Liu, Z., Fan, T., Zhou, H., Zhang, D., Gong, X., Guo, Q., et al. (2007). Synthesis of $ZnFe_2O_4$/SiO_2 composites derived from a diatomite template. Bioinspir. Biomim. *2*, 30–35.

55. Tamames-Tabar, C., Cunha, D., Imbuluzqueta, E., Ragon, F., Serre, C., Blanco-Prieto, M.J., and Horcajada, P. (2014). Cytotoxicity of nanoscaled metal–organic frameworks. J. Mater. Chem. B *2*, 262–271.

56. Ruyra, À., Yazdi, A., Espín, J., Carné-Sánchez, A., Roher, N., Lorenzo, J., Imaz, I., and Maspoch, D. (2015). Synthesis, culture medium stability, and in vitro and in vivo zebrafish embryo toxicity of metal-organic framework nanoparticles. Chemistry *21*, 2508–2518.

57. Abánades Lázaro, I., Haddad, S., Rodrigo-Muñoz, J.M., Marshall, R.J., Sastre, B., Del Pozo, V., Fairen-Jimenez, D., and Forgan, R.S. (2018). Surface-functionalization of Zr-fumarate MOF for selective cytotoxicity and immune system compatibility in nanoscale drug delivery. ACS Appl. Mater. Interfaces *10*, 31146–31157.

58. Liu, S., Ono, R.J., Wu, H., Teo, J.Y., Liang, Z.C., Xu, K., Zhang, M., Zhong, G., Tan, J.P., Ng, M., et al. (2017). Highly potent antimicrobial polyionenes with rapid killing kinetics, skin biocompatibility and in vivo bactericidal activity. Biomaterials *127*, 36–48.

59. Fiebelkorn, K.R., Crawford, S.A., McElmeel, M.L., and Jorgensen, J.H. (2003). Practical disk diffusion method for detection of inducible clindamycin resistance in *Staphylococcus aureus* and coagulase-negative staphylococci. J. Clin. Microbiol. *41*, 4740–4744.

60. Chen, Y., Hong, S., Fu, C.W., Hoang, T., Li, X., Valencia, V., Zhang, Z., Perman, J.A., and Ma, S. (2017). Investigation of the mesoporous metal–organic framework as a new platform to study the transport phenomena of biomolecules. ACS Appl. Mater. Interfaces *9*, 10874–10881.

61. Touitou, E., Dayan, N., Bergelson, L., Godin, B., and Eliaz, M. (2000). Ethosomes—novel vesicular carriers for enhanced delivery: characterization and skin penetration properties. J. Control. Release *65*, 403–418.